



Research paper

Electric Vehicle Battery Charging Using a Non-Isolated Bidirectional DC-DC Converter Connected to T-Type Three Level Converter

F. Sedaghati^{*}, S. A. Azimi

Department of Electrical Engineering, Faculty of Engineering, University of Mohaghegh Ardabili, Ardabil, Iran.

Article Info

Article History:

Received 30 June 2024
Reviewed 27 July 2024
Revised 07 September 2024
Accepted 14 September 2024

Keywords:

Electric vehicle
Battery charger
Non-isolated bidirectional dc-dc converter
T-type three-level converter
Charging station

^{*}Corresponding Author's Email Address:

farzad.sedaghati@uma.ac.ir

Abstract

Background and Objectives: Increasing environmental problems have led to the spread of Electric Vehicles (EVs). One of the attractive research fields of electric vehicles is the charging battery of this strategic product. Electric vehicle battery chargers often lack bidirectional power flow and the flexibility to handle a wide range of battery voltages. This study proposes a non-isolated bidirectional DC-DC converter connected to a T-type converter with a reduced number of switches to solve this limitation.

Methods: The proposed converter uses a DC-DC converter that has an interleaved structure along with a three-level T-type converter with a reduced number of switches and a common ground for the input and output terminals. Space vector pulse width modulation (SVPWM) and carrier based sinusoidal pulse width modulation (CBPWM) control the converter for Vehicle to grid (V2G) and grid to Vehicle (G2V) operation, respectively.

Results: Theoretical analysis shows 96.9% efficiency for 15.8kW output power and 3.06% THD during charging with low battery voltage ripple. In V2G mode, it achieves an efficiency of 96.5% while injecting 0.5 kW of power into the 380 V 50 Hz grid. The DC link voltage is stabilized. The proposed converter also provides good performance for a wide range of battery development.

Conclusion: The proposed converter offers high efficiency and cost reduction. It provides the possibility of charging a wide range of batteries and provides V2G and G2V power flow performance. The proposed converter is capable of being placed in the fast battery charging category. The ability to charge two batteries makes it a suitable option for charging stations.

This work is distributed under the CC BY license (<http://creativecommons.org/licenses/by/4.0/>)



Introduction

Electric vehicles (EV) play an important role in transportation and automotive related markets. The expansion of electric vehicles (EVs) is an ongoing trend in today's society, with the EV market growing at a very fast rate [1]. Therefore, to fully employ the potentially great number of EVs, proper charging infrastructure is a necessity [2]. This is especially crucial in terms of the ability to charge the EVs rapidly, e.g., on highways, where the utilization of highly-performant fast and ultra-fast

charging stations is required. There is a large variety of approaches that can be employed to construct fast charging stations that differ in the voltage levels, the presence of additional battery energy storage, as well as the grid structure (unipolar vs. bipolar) [3], [4]. Here, an EV charging system with a bipolar DC grid with +/- 750 V and extra battery energy storage is considered, as such a system is considered advantageous compared to more conventional approaches [5]-[7]. Increasing demand in the transportation industry with electric vehicles requires a suitable charging infrastructure for this demand.

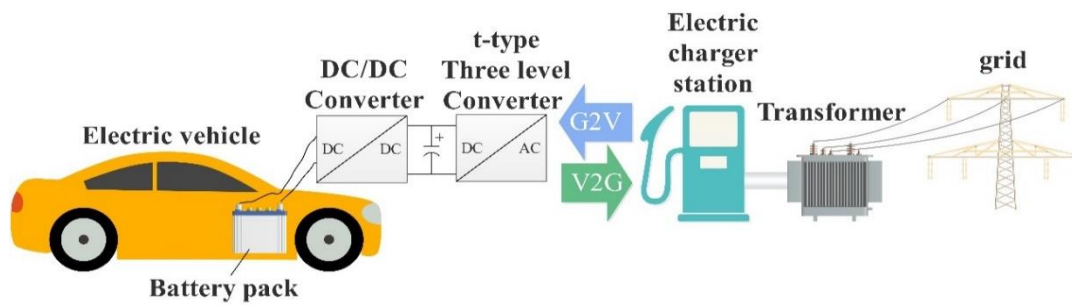


Fig. 1: Process of G2V and V2G.

However, the cost and charging time of the battery in an electric vehicle are two main issues that continue to challenge the wider application of EVs [8]. Both issues are directly related to the charging system for EVs. For example, compared to the fossil fuel station, in EV charging stations, the charging time with the battery is longer than recharging an internal combustion car, which can be balanced in the time and construction costs with the optimal design of the charger circuits. Therefore, for the development of EV applications, it is necessary to improve the charger system, especially for the off-board fast charger. In addition to solving the challenges of battery charging time and manufacturing cost, the optimal design of charger circuits should also provide power flow in two directions (V2G) and (G2V). Fig. 1 shows the process of (V2G) and (G2V). The power density can be increased by increasing the switching frequency and integrating the DC-DC converter together in an interleaved form, magnetic integration technique and introducing a single-stage approach [9]. When the battery interface converter required to connect the station’s DC-link and the battery energy storage is considered, a number of topologies can be used [10], [11]. The three-level topology provides the possibility to employ well-performing off-the-shelf 1.2 kV SiC MOSFETs and obtain lower power losses compared to other approaches [12], as well as the option to balance the DC grid [13] with low general complexity. Moreover, the interleaved two phase topology shows good perspective in terms of low output ripples [14], [15], especially important for cooperating with a battery energy storage.

Some charger topologies are suitable for a small range of output voltages. However, advanced EV chargers with wide output voltage ranges have been discussed in [16].

In [17], an EV charger based on Vienna converter is

presented.

The wide output voltage range is the main advantage of the topology, stated by the authors. It is noteworthy that most existing chargers, regardless of their single or two-stage power processing structures, use line frequency or high frequency transformers. However, transformers not only affect the cost and size of the charger but also, increase the voltage stress across semiconductor devices and reduce efficiency. Due to these disadvantages and motivated by the concept of integrated chargers [18], few researchers have demonstrated the configuration of transformer less chargers for EVs applications [19]. Researchers in [20]-[22] introduced some converters for wide ranges of output voltage in order to cover the wide variety of battery voltage from different car manufacturers. On-board battery chargers are generally lightweight and compact and have less power. But in electric charging stations, they are bulky chargers which have high weight. Therefore, the Off-board battery charging time is less than the On-board type [23], [24]. Electric vehicle batteries can help the reliability and stability of the power grid by storing energy in times of low demand and delivering power in times of peak load to the power grid.

Therefore, bidirectional chargers are important parts in these system [25]-[27].

The most advanced unidirectional battery chargers are focused on increasing power density, which has advantages such as high efficiency. The topology presented in [28] is suitable for a very high voltage battery where the aforementioned EV charger is unidirectional. Existing charging solutions for EVs with very low power factor sometimes work below 0.85. In addition, it makes the total harmonic distortion of the supply current worse [29]. So, at the full load of the charging stations, it

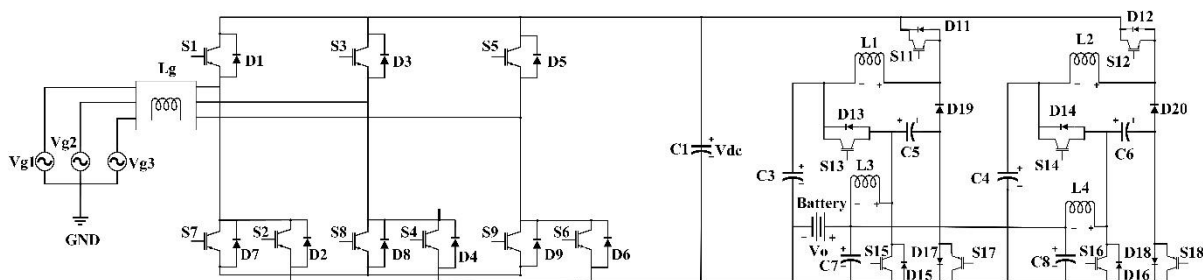


Fig. 2: Proposed charger configuration.

affects other local loads. High efficiency is required to reduce heatsink size and increase mileage per charge.

To reduce conduction losses at high load current, DC-DC converters are designed in parallel configuration for EV [30]. Due to limitation of voltage increase in the switches because of addition of leakage inductances and magnetic interference in the EMI filter and the large number of switches in the circuit, which increases the cost and reduce the efficiency of power converters. Having a common ground between the input and output ports avoids additional dv/dt problem, which is beneficial for the performance of the power converters.

This paper proposes a configuration for use in V2G and G2V applications using a bidirectional converter as an interface. The suggested configuration has good voltage gain, the low power stress in semiconductor devices, and simple structure for implementation. The converter can use switches with low rated power due to the interleaved configuration also, the proposed structure can be suitable for battery charging station and have good performance. Covering a wide range of battery voltage is one of the features of the DC-DC converter. The battery charger can charge a 380V and 40 Amp-Hour battery from 20% to 80% of State of Charge (SOC) in less than 38 minutes. The proposed configuration includes T-type three-level reduced switches converter, which is a two-way power flow AC-DC converter. In section 3, the proposed configuration is described in detail. Section 4 illustrates DC-DC converter topology and its operation. In the next sections, the control system is studied and then, the results obtained from simulations are reviewed. Finally, the last section includes conclusions.

Configuration of Proposed Charger

Fig. 2 shows the proposed charger configuration. A T-type three-level PWM converter is employed for grid-connection application. On the AC side, the three-phase voltage source is connected to the output of the three-level T-type PWM converter through an inductor filter, L_g . The AC side converter consists of nine power switches, which has three switches less than the conventional T-type three-level PWM converter. In the DC link, a capacitor whose voltage is fixed at 600 V is used. When power flows from the power grid to the DC side, switches S2, S4, and S6 are off. Also, when power flows from the DC side to the power grid, switches S7, S8 and S9 are off.

A. G2V Operation

For the power flow from the power grid to DC side, the switches of one leg are turned on and off complementary using sinusoidal pulse width modulation (SPWM) technique. Fig. 3 shows the simplified schematic of the proposed converter control, where i_{abc} and V_{abc} are the current and voltage of the three phases input to the converter, V_{ref} is the DC link reference voltage and V_{dc} is

the DC link voltage. The ratio of the carrier frequency to the main frequency is larger, therefore, the main component of the output voltage changes linearly with the reference voltage. Also, the output voltage frequency is equal to the reference voltage. V_{ref} for a constant DC link voltage from the following equation:

$$V_{out} = V_{ref} \left(\sin(\omega t) + \sin\left(\omega t + \frac{2\pi}{3}\right) + \sin\left(\omega t + \frac{4\pi}{3}\right) \right) \quad (1)$$

The output voltage can be written in term of modulation index MI, as follows:

$$V_{out} = \frac{V_{dc}}{2} MI \left(\sin(\omega t) + \sin\left(\omega t + \frac{2\pi}{3}\right) + \sin\left(\omega t + \frac{4\pi}{3}\right) \right) \quad (2)$$

So, $V_{ref} < V_{dc}/2$ and $0 < MI < 1$. SPWM, which are used to stabilize the DC link voltage at 600 volts and transfer power from the grid to DC. Voltages A_n , B_n and C_n vary between two values $V_{dc}/2$ and $-V_{dc}/2$. In this mode, T-type three-level PWM converter operates like the Vienna rectifier, and diodes D1, D2, D3, D4, D5 and D6 conduct. Also, switches S1, S2, S3, S4, S5 and S6 will be turned off. It should be noted that turning on the top three switches in each leg reduces the voltage of the current passing through the top diodes of each leg.

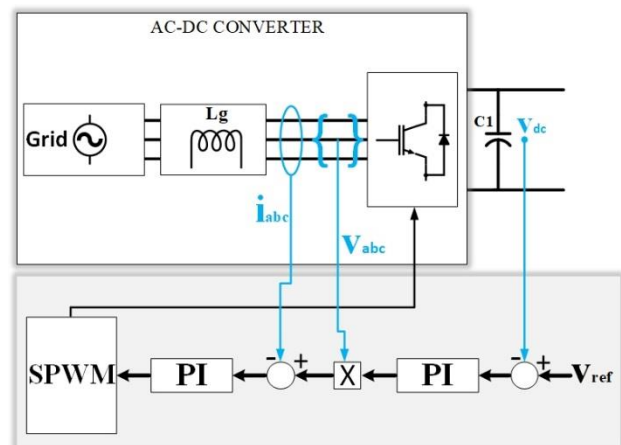


Fig. 3: Simplified schematic of AC-DC Converter with controller for G2V operation.

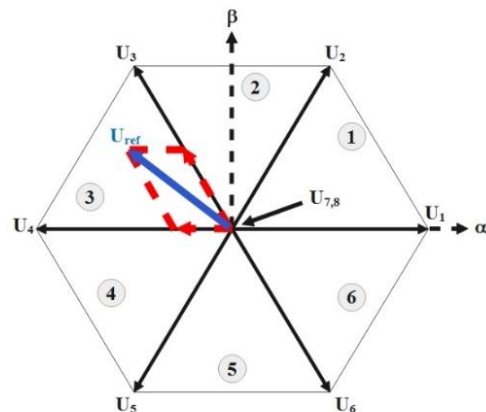


Fig. 4: Space vector diagram.

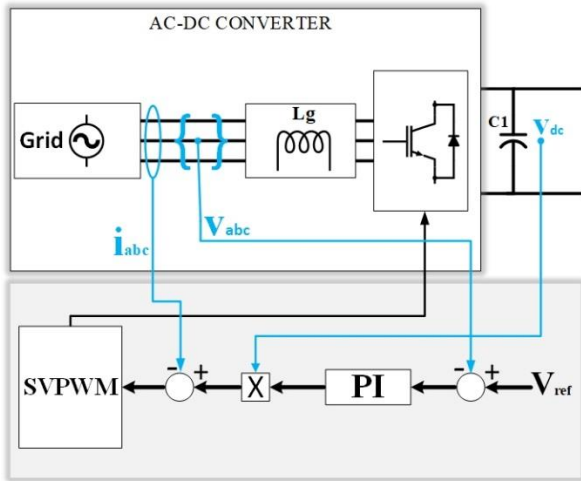


Fig. 5: Simplified schematic of AC-DC Converter with controller for V2G operation.

Table 1: State of top switches

Vector	S1	S3	S5
U1	1	0	0
U2	1	1	0
U3	0	1	0
U4	0	1	1
U5	0	0	1
U6	1	0	1
U7	0	0	0
U8	1	1	1

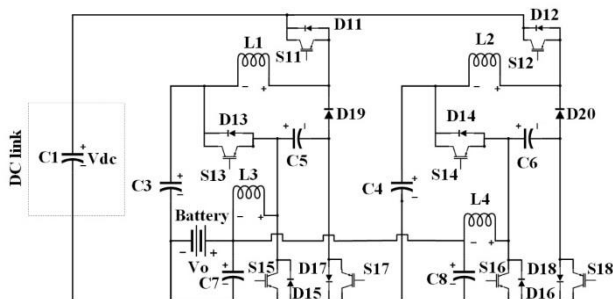


Fig. 6: Proposed DC-DC Conversion system.

B. V2G Operation

In this working mode, power flows from the electric vehicle to the grid. Therefore, the performance of the converter will be the same as a 3-phase inverter. A constant voltage to a three-phase sinusoidal voltage should be provided for the network. Switches S1-S6 are active in directing power from the DC side to the grid.

Space Vector Pulse Width Modulation (SVPWM) control method is applied to reduce switching losses, reduce harmonic distortion and also, use DC link terminal voltage properly. SVPWM can be used to generate pulses for three-phase two-level DC-AC converters. the reference vector U_{ref} is averaged using two adjacent space vectors (U3 and U4 in the Fig. 4) for a given period and a null vector (U7 or U8) for the rest of the period. Fig. 5

shows a simple schematic and controller for V2G operation of T-type converter. Table 1 shows the state of the top switches of each leg for each vector. Eight switching modes, including six active modes and two zero modes, are available. These vectors form a hexagon (Figure 4), which can be seen as consisting of six sections at 60 degrees. The reference vector representing the three-phase sinusoidal voltage is generated using SVPWM by switching between the two nearest active vectors and the zero vector. The sinusoidal reference space vector forms a circular path inside the hexagon. The largest output voltage value that can be obtained using SVPWM is the radius of the largest circle that can be recorded in the hexagon. This circle is tangent to the midpoints of the lines that join the ends of the active space vector. Finally, the model of a three-phase inverter based on space vector representation enables the proposed converter to deliver power from the battery to the grid.

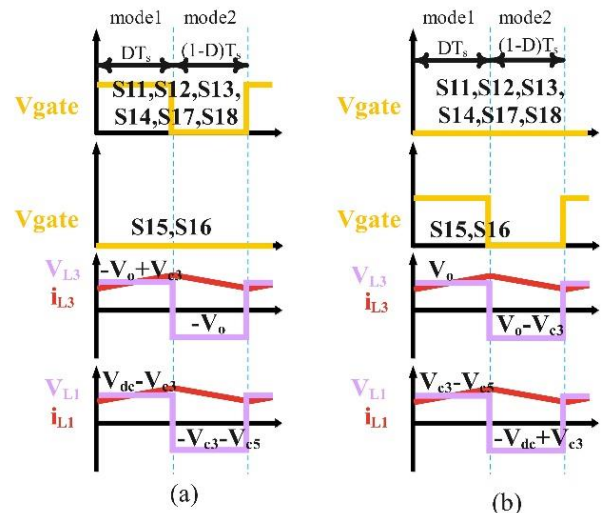


Fig. 7: Time-domain waveforms in CCM: (a) G2V, (b) V2G.

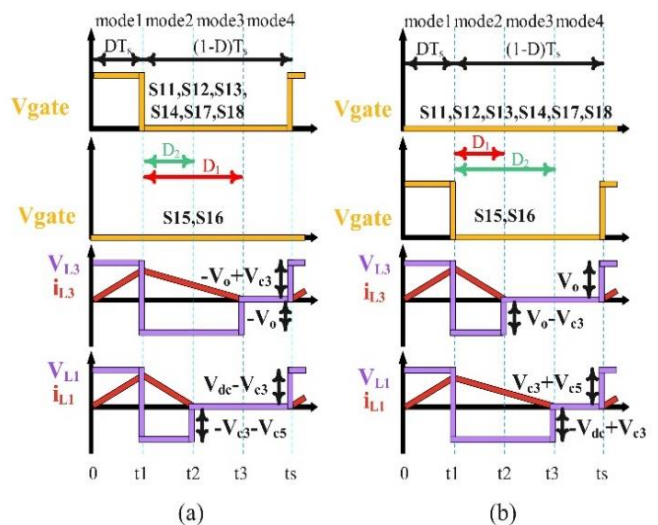


Fig. 8: Time-domain waveforms in DCM operation: (a) G2V, (b) V2G.

DC-DC Conversion

Fig. 6 shows the configuration of the proposed DC-DC conversion system. The DC-DC converter is connected to battery on one side and to the DC link on the other side. V_o and V_{dc} show the battery and the DC link voltages, respectively. Interleaved DC-DC converter is proposed to reduce the voltage and current stress and, increase the reliability of the DC-DC conversion. Therefore, we will only examine the first part of the DC-DC converter. The proposed converter consists of four inductors L1, L2, L3, and L4, four capacitors C1, C2, C3, and C4, eight switches S11, S12, S13, S14, S15, S16, S17, and S18 and ten diodes D11, D12, D13, D14, D15, D16, D17, D18, D19 and D20. Body switches and diodes conduct complementary during a complete switching period (T_s). The V2G and G2V working modes of the DC-DC converter in continuous conduction mode (CCM) and discontinuous conduction mode (DCM) are shown in Fig. 7 and Fig. 8, and the detailed analysis of each mode is given in the following.

A. G2V Operation

Two modes for CCM operation and four modes for DCM are defined as follow:

The first mode of CCM and DCM [0- t_1]: according to Fig. 9(a), switches S11, S13 and S17 are turned on and switch S15 is off. In this time interval, inductor L1 is charged by the input DC link and the energy released from capacitor C3. Therefore, the current through inductor L1 increases, while inductor L3 is energized from C5. The derived current and voltage equations according to the time-domain waveform in Fig. 8(a) are:

$$\begin{cases} v_{L1} = L_1 \frac{di_{L1}}{dt} = V_{dc} - V_{C3} = V_{dc} - V_{C5} \\ v_{L3} = L_3 \frac{di_{L3}}{dt} = -V_o + V_{C3} = -V_o + V_{C5} \end{cases} \quad (3)$$

the voltage of two capacitors C3 and C5 are equal.

The second mode of CCM [t_1 - T_s] and DCM [t_1 - t_2]: unlike the first mode, according to Fig. 9(b), while diodes D15 and D19 conduct, switches S11, S13 and S15 are turned off. Inductor L1 gives its energy to capacitors C3 and C5. Also, the energy of inductor L3 is discharged.

$$\begin{cases} v_{L1} = L_1 \frac{di_{L1}}{dt} = -V_{C3} - V_{C5} \\ v_{L3} = L_3 \frac{di_{L3}}{dt} = -V_o \end{cases} \quad (4)$$

Applying volt-second balance law on inductors L1 and L2 yields:

$$D(V_{dc} - V_{C3}) + (1-D)(-V_{C3} - V_{C5}) = 0 \quad (5)$$

$$D(-V_o + V_{C3}) + (1-D)(-V_o) = 0 \quad (6)$$

D stands for duty cycle. Using (6), the average voltage on the capacitors C3 and C5 are calculated as follows:

$$V_{C3} = V_{C5} = V_o / D \quad (7)$$

The voltage conversion ratio of the proposed converter during CCM operation for G2V mode is obtained from (6) and (7) as follows:

$$M_{G2V(CCM)} = \frac{V_o}{V_{dc}} = \frac{D^2}{2 - D} \quad (8)$$

The third mode of DCM [t_2 - t_3]: in this state, the current passing through inductor L1 in t_2 and the current passing through inductor L3 in t_3 reach zero.

The fourth mode of DCM [t_3 - T_s]: in this state, the current through the inductors reaches zero and all the switches are off. A full cycle of T_s is completed at the end of this interval. Diodes D1 and D2 can be defined as duty cycles where the current through the inductors becomes zero. Therefore, according to the Fig. 9(c), the voltages across the inductors are given as follow:

$$V_{L1} = \begin{cases} V_{dc} - V_{C3} & 0 \leq t < DT_s \\ -V_{C3} - V_{C5} & DT_s \leq t < (D + D_2)T_s \\ 0 & (D + D_2)T_s \leq t < T_s \end{cases} \quad (9)$$

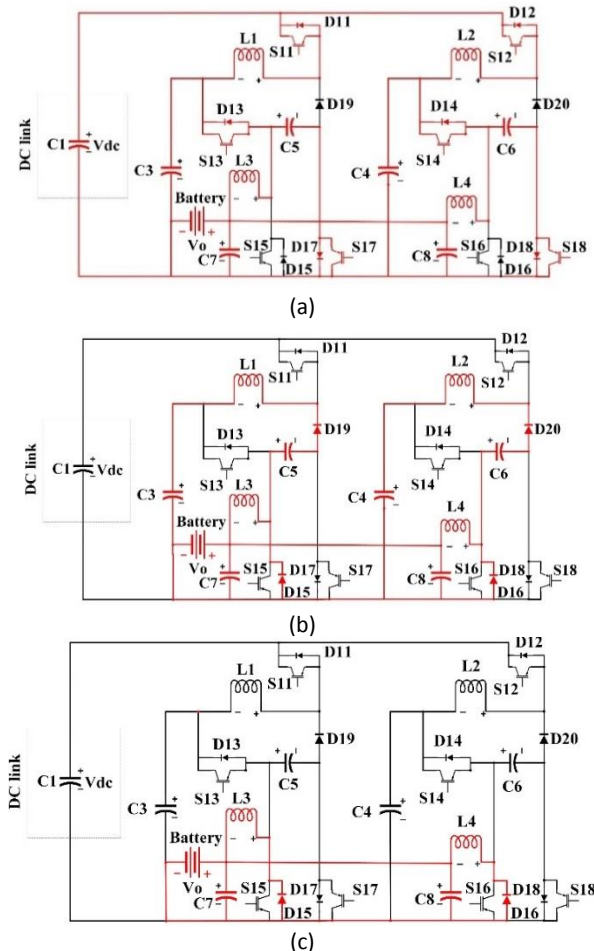


Fig. 9: Equivalent circuit of the proposed DC-DC converter in G2V operation: (a) Mode 1, (b) Mode 2, (c) Mode 3.

$$V_{L3} = \begin{cases} -V_o + v_{C3} & 0 \leq t < DT_s \\ -V_o & DT_s \leq t < (D + D_1)T_s \\ 0 & (D + D_1)T_s \leq t < T_s \end{cases} \quad (10)$$

By applying volt-second balance law on both inductors, voltage of capacitors is calculated as given in (16).

$$V_{C3}=V_{C5}=(D+D_1)V_0/D \quad (11)$$

So, during this mode, DCM voltage gain transfer ratio is calculated as follows:

$$M_{G2V(DCM)} = \frac{V_o}{V_{dc}} = \frac{D^2}{(D+D_1)(D+2D_2)} \quad (12)$$

B. V2G Operation

Unlike the G2V Operation mode, in this mode, the power flows from the battery side to the DC link. Two modes are defined for CCM operation and four modes for DCM:

First mode of CCM and DCM [0-t1]: in this interval, only switch S15 conducts, as shown in Fig. 10(a). The DC source charges inductors L3 and L1, that increases the current. The energy of capacitors C1 and C2 is discharged in inductor L1. Fig. 8(b) shows the derived current and voltage equation.

$$\begin{cases} v_{L1} = L_1 \frac{di_{L1}}{dt} = v_{C3} + v_{C5} \\ v_{L3} = L_3 \frac{di_{L3}}{dt} = V_0 \end{cases} \quad (13)$$

The second mode, CCM [t1-Ts] and DCM [t1-t2]: according to Fig. 10(b), only three diodes D11, D13 and D17 conduct and all switches are off. Inductor L3 discharges energy to capacitor C5, and inductor L1 discharges its energy to DC link.

$$\begin{cases} v_{L1} = L_1 \frac{di_{L1}}{dt} = -V_{dc} + v_{C3} = -V_{dc} + v_{C5} \\ v_{L3} = L_3 \frac{di_{L3}}{dt} = V_0 - v_{C3} = V_0 - v_{C5} \end{cases} \quad (14)$$

It can be seen that the voltage of capacitors C3 and C5 are equal. If we apply the volt-second balance law on the inductors, we have:

$$D(V_0) + (1-D)(V_0 - V_{C3}) = 0 \quad (15)$$

$$D(V_{C3} + V_{C5}) + (1-D)(-V_{dc} + V_{C3}) = 0 \quad (16)$$

Using (15), the voltage of capacitors C1 and C2 can be determined as follow:

$$V_{C3} = V_{C5} = \frac{V_0}{(1-D)} \quad (17)$$

The voltage conversion ratio of the proposed converter during CCM operation for V2G is obtained from (16) and (17).

$$M_{V2G(CCM)} = \frac{V_{dc}}{V_0} = \frac{1+D}{(1-D)^2} \quad (18)$$

Third mode of DCM [T2 -T3]: current of inductor L1 reaches to zero.

Fourth mode, DCM [t3-Ts]: the current through the inductors reaches to zero and all switches are off. At the end of this interval, a full switching period of Ts is

completed. As shown in Fig. 10(c), the voltages on both sides of the inductors are calculated as follow:

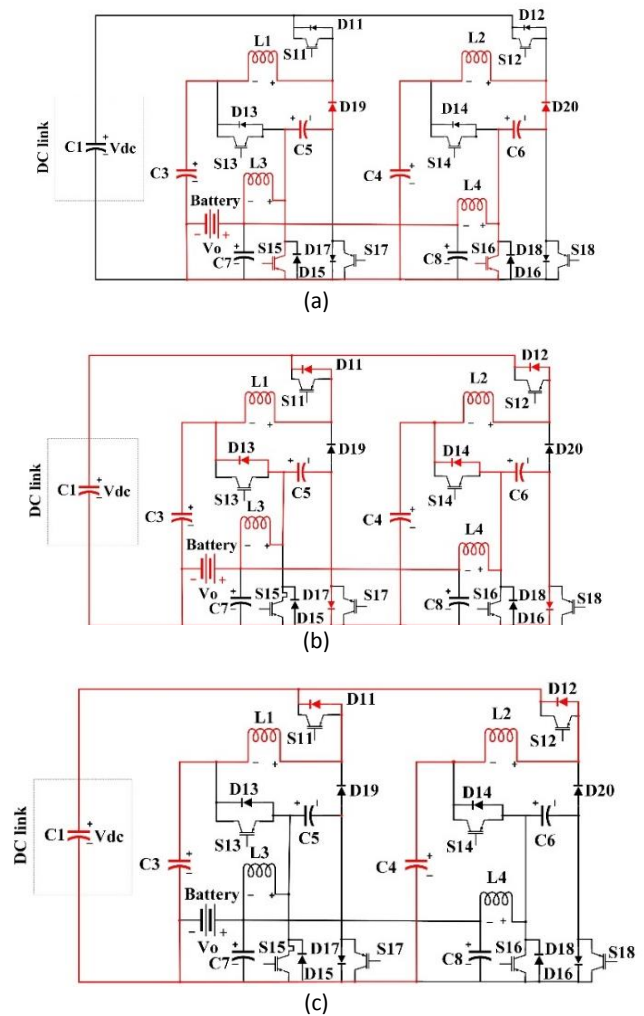


Fig. 10: Equivalent circuit of the proposed DC-DC converter in V2G operation: (a) Mode 1, (b) Mode 2, (c) Mode 3.

$$v_{L1} = \begin{cases} v_{C3} + v_{C5} & 0 \leq t < DT_s \\ -V_{dc} + v_{C3} & DT_s \leq t < (D+D_2)T_s \\ 0 & (D+D_2)T_s \leq t < Ts \end{cases} \quad (19)$$

$$v_{L3} = \begin{cases} V_0 & 0 \leq t < DT_s \\ V_0 - v_{C3} & DT_s \leq t < (D+D_1)T_s \\ 0 & (D+D_1)T_s \leq t < Ts \end{cases} \quad (20)$$

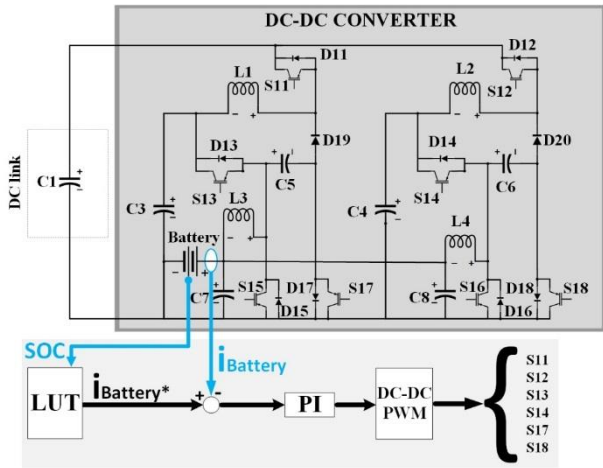
The volt-second balance law is applied to inductors L1 and L3.

Therefore, the voltages of capacitors C3 and C5 are equal to (21).

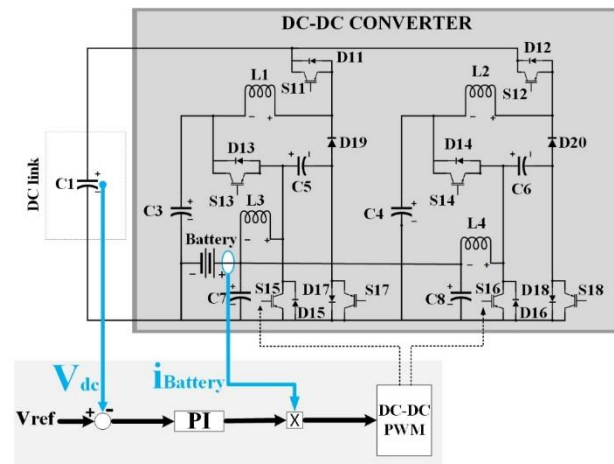
$$V_{C3} = V_{C5} = \frac{(D+D_1)V_0}{D_1} \quad (21)$$

So, the DCM voltage gain in V2G mode can be obtained as follows:

$$M_{V2G(DCM)} = \frac{V_{dc}}{V_0} = \frac{(D+D_1)(2D+D_2)}{D_1 D_2} \quad (22)$$



(a)



(b)

Fig. 11: schematic of DC-DC Converter with controller: (a) G2V, (b) V2G.

Proposed DC-DC Converter Control System

In G2V operating mode, the difference between V_{dc} and V_{ref} is given to PI controller. The PI controller output duty cycle is compared with a sawtooth wave to apply the gate pulses to the switches S15 and S16 (fig. 11(a)). During G2V operation, switches S15 and S16 are off. SOC extracts the appropriate current of $i_{Battery}^*$ using lookup table (LUT) data. The difference between $i_{Battery}$ and $i_{Battery}^*$ is given to the PI controller. The output of the PI controller determines the duty cycle (fig. 11(b)). By using PWM Generator, the required pulses are applied to switches S11, S12, S13, S14, S17 and S18 with the desired duty cycle. A 380 Volt 40 ampere-hour battery is applied in the studied system. The proposed topology can be used for a wide range of battery voltages.

Duty Cycle for G2V and V2G Operation

Using the battery and DC link voltages, it obtained that the duty cycle in G2V and V2G operation modes are calculated as follow:

$$D_{G2V} = 0.5 \left(-V_o + \sqrt{V_o^2 + 8V_o V_{dc}} \right) / V_{dc} \quad (23)$$

$$D_{V2G} = 0.5 \left(2V_{dc} + V_o - \sqrt{V_o^2 + 8V_o V_{dc}} \right) / V_{dc} \quad (24)$$

Current ripple and average current of inductors are equal to:

$$G2V: \Delta i_{L3} = \frac{1-D}{L_3 f_s} V_{dc}; \Delta i_{L1} = \frac{2(1-D)}{L_1 f_s D} V_{dc} \quad (25)$$

$$V2G: \Delta i_{L3} = \frac{D}{L_3 f_s} V_o; \Delta i_{L1} = \frac{2D}{L_1 f_s (1-D)} V_o \quad (26)$$

$$I_{L3} = I_o = \Delta i_{L3} (D + D_1) / 4 \quad (27)$$

$$I_{L1} = \frac{D}{2-D} I_o = \frac{1-D}{1+D} I_o = \Delta i_{L1} (D + D_2) / 4 \quad (28)$$

f_s is switching frequency. For DCM modes, D_1 and D_2 can be calculated as follow:

$$G2V: \begin{cases} D_1 = \frac{2L_3 f_s I_o}{(1-D)V_o} - D \\ D_2 = \frac{D^2 L_1 f_s I_o}{(2-D)(1-D)V_o} - D \end{cases} \quad (29)$$

$$V2G: \begin{cases} D_1 = \frac{2L_3 f_s I_o}{D V_o} - D \\ D_2 = \frac{(1-D)L_1 f_s I_o}{D(1+D)V_o} - D \end{cases} \quad (30)$$

Design of Passive Elements

The values of inductance are concluded from (4) and (14), as follow:

$$G2V: L_3 \geq \frac{1-D}{\Delta i_{L3} f_s} V_o; L_1 \geq \frac{2(1-D)}{\Delta i_{L1} f_s D} V_o \quad (31)$$

$$V2G: L_3 \geq \frac{D}{\Delta i_{L3} f_s} V_o; L_1 \geq \frac{2D}{\Delta i_{L1} f_s (1-D)} V_o \quad (32)$$

Table 2: Values for each element in the proposed DC-DC converter

Parameters	Values
Rated power (P_{out})	17 [KW]
Battery and DC Link side voltages (V_o, V_{dc})	380 [V] and 600 [V]
3-Phase Grid side voltage (V_g)	380 [V], 50 [Hz]
Switching frequency (f_s)	1 [kHz]
Inductors L1, L3 and L_g	1 [mH], 2.2 [mH] and 1 [mH]
Capacitors C1, C3, C5 and C7	470 [μ F], 330 [μ F], 330 [μ F] and 2.2 [μ F]

In CCM operation mode, the minimum inductor current must be positive, so the critical values of inductors are obtained as follow:

$$G2V: L_3 \geq \frac{(1-D)V_o}{2f_s I_o}; L_1 \geq \frac{(2-D)(1-D)}{D^2 f_s I_o} V_o \quad (33)$$

$$V2G: L_3 \geq \frac{D V_o}{2f_s I_o}; L_1 \geq \frac{D(1+D)V_o}{(1-D)^2 f_s I_o} \quad (34)$$

Values of capacitors are determined as follow:

$$G2V: C_{3,5} \geq \frac{D(1-D)I_o}{\Delta v_{C3,5} f_s (2-D)}; C_7 \geq \frac{(1-D)V_o}{8\Delta v_{C7} f_s^2 L_1} \quad (35)$$

$$V2G: C_{3,5} \geq \frac{D(1-D)I_o}{\Delta v_{C3,5}f_s(1+D)}; C_{dc} \geq \frac{D(1-D)^2V_o}{\Delta v_{Cdc}f_s(1+D)} \quad (36)$$

By having the allowed ripple of capacitors voltage, and considering (35) and (36), the values of capacitors are obtained. Considering the interleaved configuration of DC-DC converter, the obtained values for each element in one part is similar to the same element in the other part. Table 2 shows the values of DC-DC converter elements.

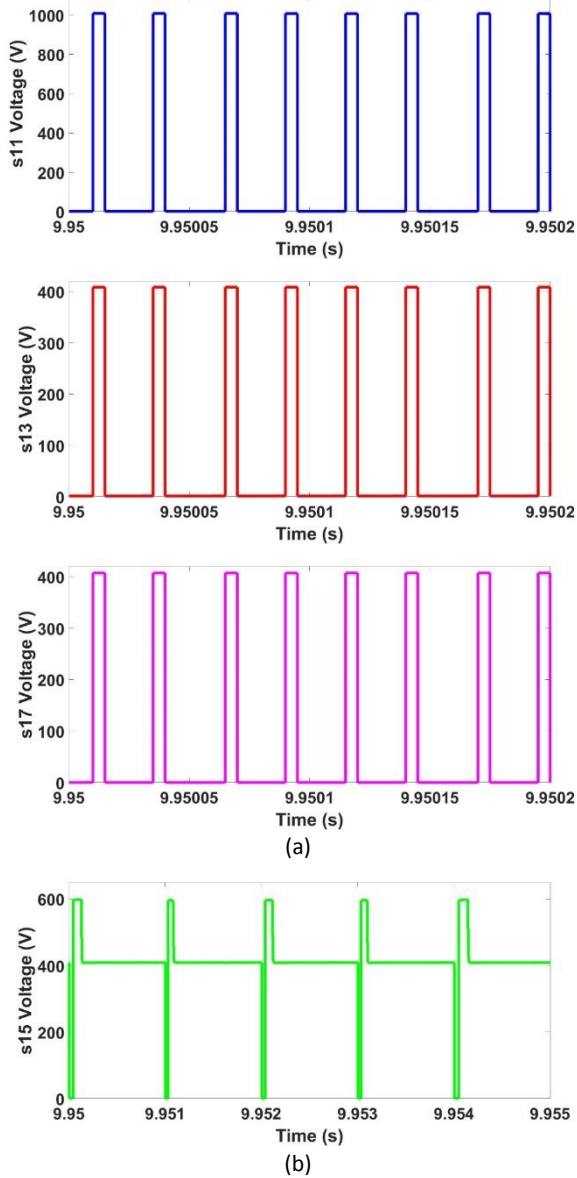


Fig. 12: The voltage of on switches: (a) G2V, (b) V2G.

Comparison

The proposed battery charger is compared with similar chargers in this section and results are given in Table. 3. As mentioned before, the proposed configuration has bidirectional power flow capability which only some of the chargers have this capability. Also, from efficiency point of view, the proposed configuration has relatively good situation. It should be noted that the ratio of the output power to the input power is used to determine the efficiency. As, in the V2G working mode the input power

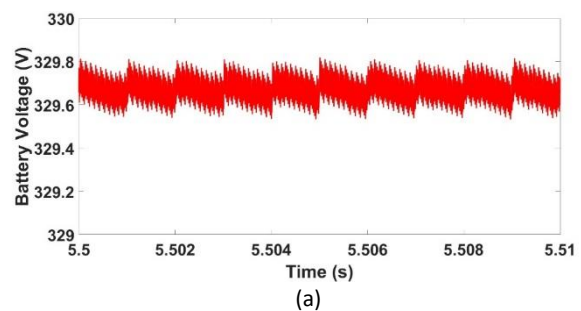
is the battery power and the power delivered to the network is the output power, and in the G2V working mode, the power to the battery is the output power and the converter power is considered as the input power. The given battery charger has the best battery voltage range among the compared chargers.

Table 3: Results of comparison between the proposed charger and similar configurations

REF.	Efficiency	Bidirectional power flow	Battery voltage range	Switching frequency
[1]	99%	No	200-650 V	20-80 kHz
[2]	97.01%	No	460-800 V	150 kHz
[4]	97.5%	Yes	48 V	10 kHz
[5]	98.4%	Yes	400 V	20 kHz
[7]	98.2%	No	150-950 V	500 kHz
[8]	95.6%	Yes	48-450 V	40 kHz
[9]	97.2%	Yes	40 V	50 kHz
[12]	99.2%	No	700-900 V	50-160 kHz
[13]	98%	Yes	430-620 V	20 kHz
[15]	97.9%	No	800 V	100 kHz
[16]	92.08%	No	46-65 V	20 kHz
[17]	96.7%	No	9-16 V	260-400 kHz
Proposed	>96%	Yes	20-600 V	1 kHz

Simulation Results

It has been designed in Simulink MATLAB software to validate the control scheme and battery topology of the proposed charger. The switching frequency is considered to be 1 kHz, and the selfie filter is 1 mH is connected to a three-phase network of 380 V and 50 Hz. In this simulation, a battery with a voltage of 380 volts and a current of 40 amp-hours is used, which can be replaced with different batteries with different voltage-current ranges. Fig. 12(a) in CCM mode shows the voltage of switches S11, S13 and S17 in G2V mode, which are “on” in this mode. Fig. 12(b) shows the voltage of switch S15 in DCM mode and in V2G mode. The voltages of other switches are the same as the corresponding interleaved switch. In CCM mode and in G2V operation mode, according to Fig. 13(a), Battery voltage ripple is less than one volt. Fig. 13(b) shows the charging current of the battery in full load.



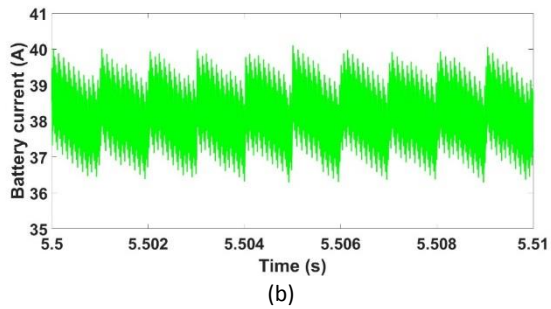


Fig. 13: CCM operation in G2V: (a) Battery voltage, (b) Battery current.

The ripple of the battery charging current is less than 4 amps. In DCM mode and V2G operation mode, battery discharge voltage and current are shown as shown in Fig. 14.

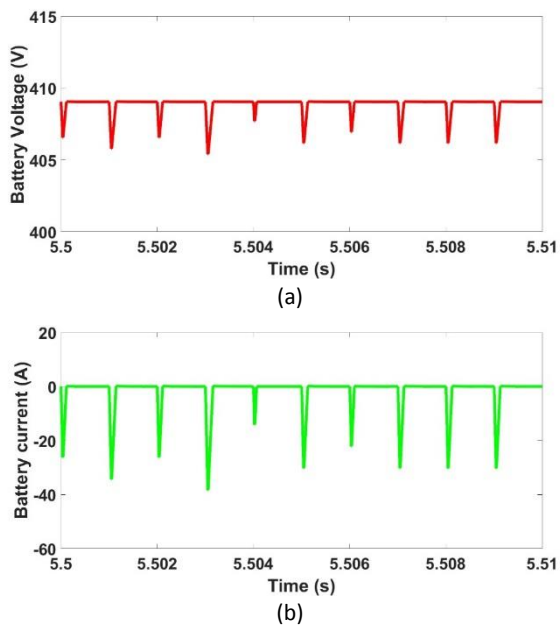


Fig. 14: DCM operation in V2G: (a) Battery voltage, (b) Battery current.

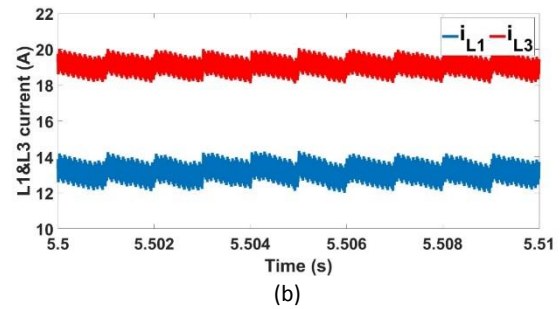
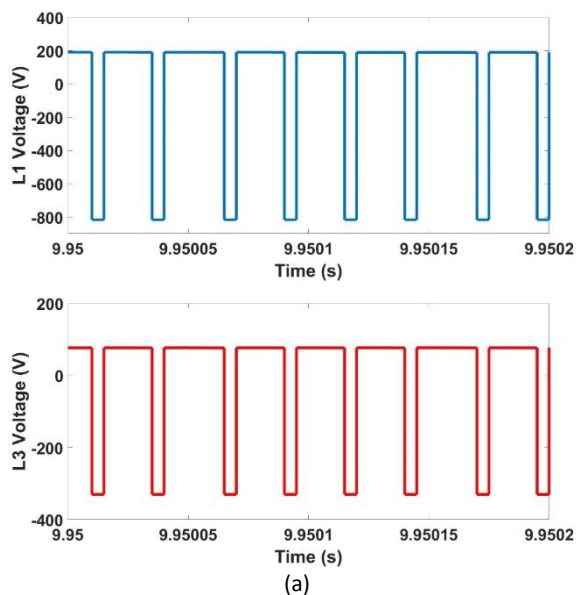


Fig. 15: Inductor voltage, and (b) inductor current in CCM mode.

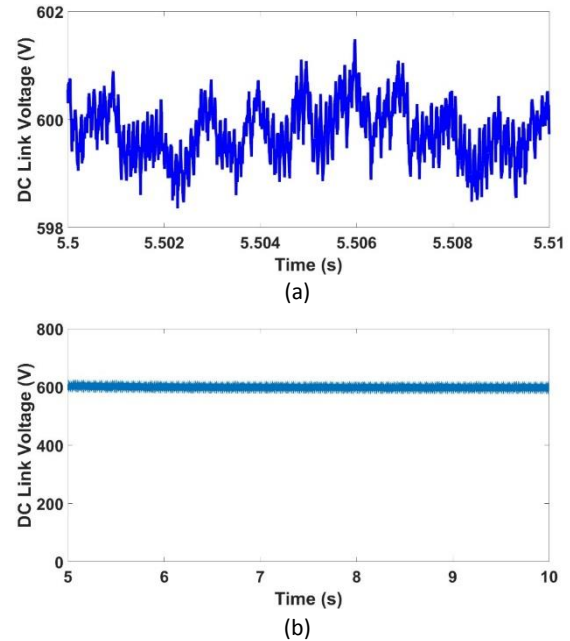


Fig. 16: DC Link voltage: (a) G2V, (b) V2G.

Fig. 15 shows the voltage and current of inductors L1 and L3 in G2V operation mode. The current ripple of the inductors is about 2 amps. Also, DC link voltage in G2V and V2G operation modes are given in Fig. 16. In the V2G operation mode, the voltage and current of the inductors for 0.5kW load on the network side are shown in Fig. 17.

The reference voltage for the DC link is 600 volts, which shows a ripple of less than 4 volts for G2V operation mode. By connecting a load of 380V and 500W, the phase-to-phase voltage and the current waveform of phase A are obtained as shown in Fig. 18.

In order to check the usability of the proposed converter in charging stations, two DC-DC converters are connected to the DC link in parallel. This type of connection provides the ability to charge an electric vehicle with only one AC-DC converter, which will ultimately lead to a reduction in the number of elements and cost, but also can charge cars with different battery capacities at the same time.

Fig. 19 shows the charging current of two identical batteries that have the same SOCs. The current ripple of both batteries is equal and varies from 36 to 41 amps.

Assuming that these 2 electric cars are charging, the current of phase A is shown in Fig. 20.

The peak of this current depends on the number of EVs being charged and the SOC of the batteries. According to the obtained simulation results, the proposed converter can be placed in the category of off-board fast charger, which can charge a 380 volt and 40 amp-hour battery in less than 38 minutes. The peak of this current depends on the number of EVs being charged and the SOC of the batteries.

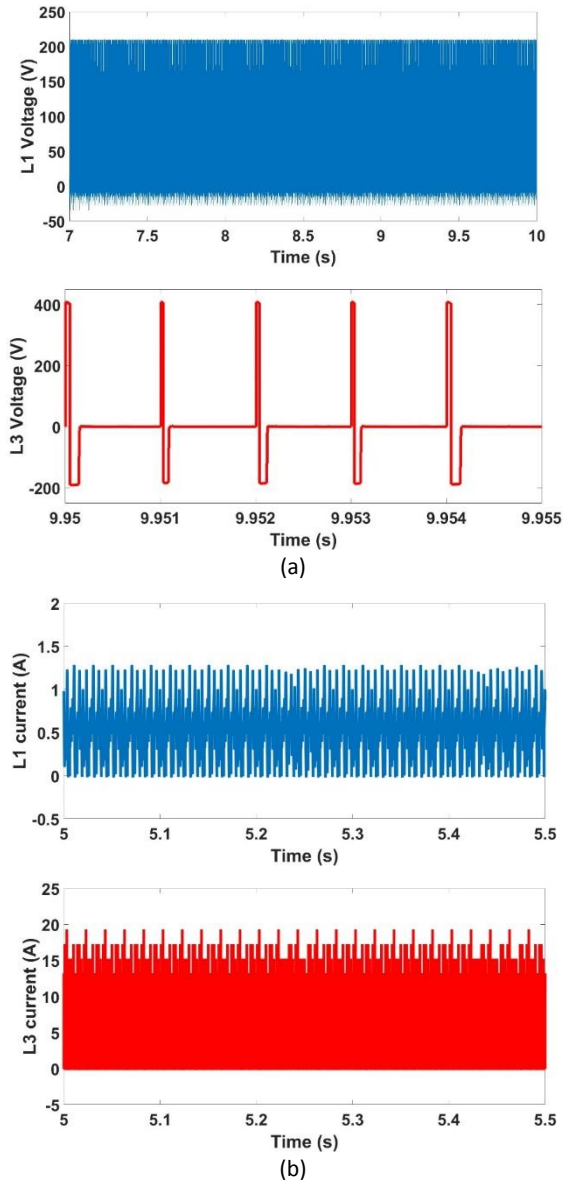


Fig. 17: (a) Inductor voltage, and (b) inductor current in DCM mode.

According to the obtained simulation results, the proposed converter can be placed in the category of off-board fast charger, which can charge a 380 volt and 40 amp-hour battery in less than 38 minutes. Fig. 21 illustrates power factor variations in the grid side of the proposed battery charger. As shown in this figure, power factor is nearly unit during the charge process.

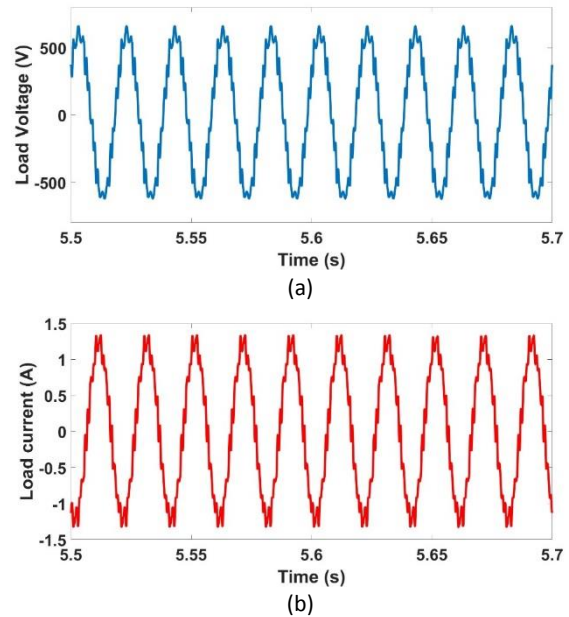


Fig. 18: Load voltage and current: (a) Phase to Phase Voltage, (b) Phase A current.

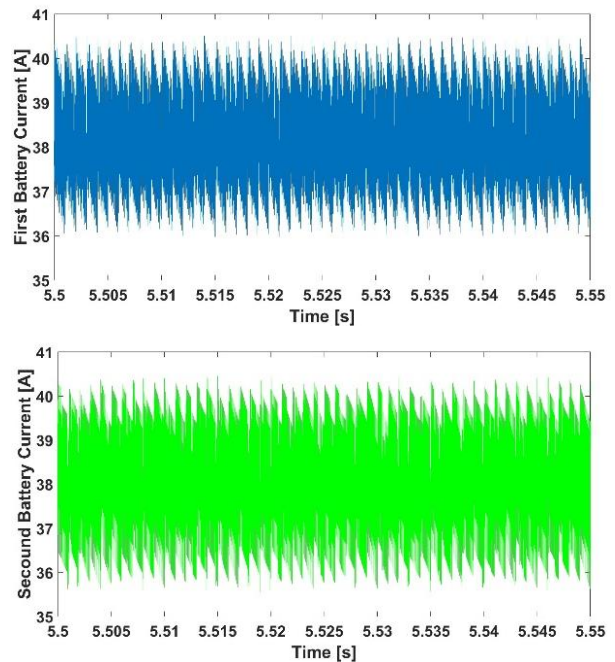


Fig. 19: The current of Batteries in the charging station.

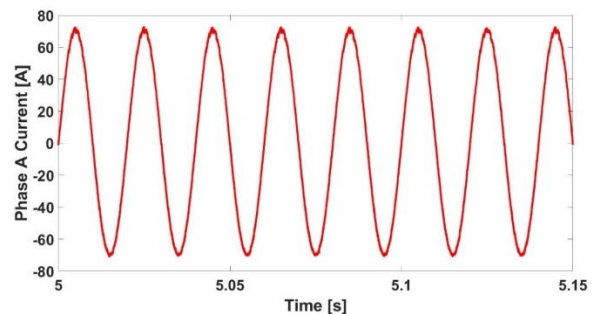


Fig. 20: Phase A current when connecting to two electric vehicles.

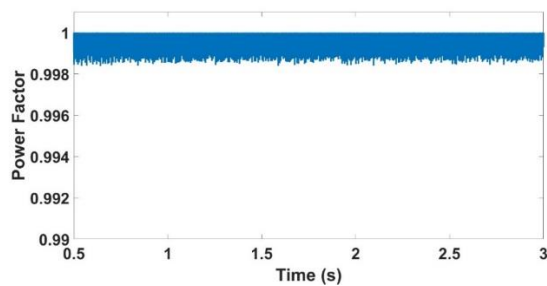


Fig. 21: Power factor variation during charge process.

Conclusions

In this paper, a non-isolated bidirectional DC-DC converter connected to a T-type three level converter for V2G and G2V applications is presented. The number of keys of the proposed T-type converter is reduced compared to the conventional T-type converter, which leads to a cost reduction in this structure. The proposed configuration has the merits of a common ground and ability of flow power in both directions. The low harmonic distortion of this structure is about 3%. In order to stabilize the DC link voltage, this structure uses SVPWM controller in V2G operation and SPWM controller in reverse power flow mode. The battery charger can charge a 380V and 40 amp-hour battery from 20-80% of SOC in less than 38 minutes that shows the charger operates as a fast charger. The proposed battery charger can be used in the charging station for a wide range of batteries with different voltages and currents. The advantages make the proposed converter one of the suitable options for battery chargers for electric vehicles.

Author Contributions

F. Sedaghati chose the field of research. S. A. Azimi collected information in this field. F. Sedaghati presented the proposed structure. S. A. Azimi simulated and controlled the proposed converter structure in MATLAB software. The authors discussed the obtained results and drew conclusions. Under the supervision of F. Sadaghti, the text of the article was prepared by S. A. Azimi. F. Sedaghati uploaded the article.

Acknowledgment

I appreciate the referees and their colleagues who helped the authors in publishing this article.

Conflict of Interest

The authors declare no potential conflict of interest regarding the publication of this work. In addition, the ethical issues including plagiarism, informed consent, misconduct, data fabrication and, or falsification, double publication and, or submission, and redundancy have been completely witnessed by the authors.

Abbreviations

<i>EV</i>	Electric Vehicle
<i>SVPWM</i>	Space Vector Pulse Width Modulation

<i>CBPWM</i>	Carrier Based Sinusoidal Pulse Width Modulation
<i>V2G</i>	Vehicle to grid
<i>G2V</i>	grid to Vehicle
<i>THD</i>	Total Harmonic Distortion
<i>SOC</i>	State of Charge
<i>SPWM</i>	Sinusoidal Pulse Width Modulation
<i>CCM</i>	Continuous Current Mode
<i>DCM</i>	Discontinuous Current Mode

References

- [1] A. Ghosh, "Possibilities and challenges for the inclusion of the Electric Vehicle (EV) to reduce the carbon footprint in the transport sector: A review," *Energies*, 13(10): 1-22, 2020.
- [2] A. Hussain, V. H. Bui, J. W. Baek, H. M. Kim, "Stationary energy storage system for fast ev charging stations: Simultaneous sizing of battery and converter," *Energies*, 12(23): 1-17, 2019.
- [3] S. Rivera, R. L. F. S. Kouro, T. Dragičević, B. Wu, "Bipolar DC power conversion: State-of-the-art and emerging technologies," *IEEE J. Emerg. Sel. Top. Power Electron.*, 9(2): 1192-1204, 2020.
- [4] M. A. H. Rafi, J. Bauman, "A comprehensive review of DC fast-charging stations with energy storage: Architectures, power converters, and analysis," *IEEE Trans. Transp. Electrification*, 7(2): 345-368, 2021.
- [5] S. Rivera, B. Wu, "Electric vehicle charging station with an energy storage stage for Split-DC bus voltage balancing," *IEEE Trans. Power Electron.*, 32(3): 2376-2386, 2016.
- [6] I. Aghabali, J. Bauman, P. J. Kollmeyer, Y. Wang, B. Bilgin, A. Emadi, "800-V electric vehicle powertrains: Review and analysis of benefits, challenges, and future trends," *IEEE Trans. Transp. Electrification*, 7(3): 927-948, 2021.
- [7] Y. Tahir et al., "A state-of-the-art review on topologies and control techniques of solid-state transformers for electric vehicle extreme fast charging," *IET Power Electron.*, 14(9): 1560-1561, 2021.
- [8] L. Zhou, M. Jahnes, M. Eull, W. Wang, M. Preindl, "Control design of a 99% efficiency transformerless EV charger providing standardized grid services," *IEEE Trans. Power Electron.*, 37(4): 4022-4038, 2022.
- [9] H. Kim, J. Park, S. Kim, R. M. Hakim, H. Belkamel, S. Choi, "A single-stage electrolytic capacitor-less EV charger with single- and three-phase compatibility," *IEEE Trans. Power Electron.*, 37(6): 6780-6791, 2022.
- [10] Y. Du, X. Zhou, S. Bai, S. Lukic, A. Huang, "Review of nonisolated bidirectional DC-DC converters for plug-in hybrid electric vehicle charge station application at municipal parking decks," in *Proc. 2010 Twenty-Fifth Annual IEEE Applied Power Electronics Conference and Exposition (APEC)*: 1145-1151, 2010.
- [11] P. Falkowski, M. Korzeniewski, A. Ruszczyc, K. Kóska, "Analysis and design of high efficiency DC/DC buck converter," *Przegląd Elektrotechniczny*, 5: 150-156, 2016.
- [12] S. Dusmez, A. Hasanzadeh, A. Khaligh, "Loss analysis of non-isolated bidirectional DC/DC converters for hybrid energy storage system in EVs," in *Proc. 2014 IEEE 23rd International Symposium on Industrial Electronics (ISIE)*: 543-549, 2014.
- [13] L. Tan, B. Wu, V. Yaramasu, S. Rivera, X. Guo, "Effective voltage balance control for bipolar-DC-bus-fed EV charging station with three-level DC-DC fast charger," *IEEE Trans. Ind. Electron.*, 63(7): 4031-4041, 2016.
- [14] V. Monteiro, J. C. Ferreira, A. A. N. Meléndez, C. Couto, J. L. Afonso, "Experimental validation of a novel architecture based on a dual-stage converter for off-board fast battery chargers of electric vehicles," *IEEE Trans. Veh. Technol.*, 67(2): 1000-1011, 2018.

[15] S. Lu, M. Mu, Y. Jiao, F. C. Lee, Z. Zhao, "Coupled inductors in interleaved multiphase three-level DC-DC converter for high-power applications," *IEEE Trans. Power Electron*, 31(1): 120-134, 2016.

[16] S. Utsav, B. Singh, "A bidirectional battery charger for a wide range of electric vehicles," in *Proc. 2022 IEEE Global Conference on Computing, Power and Communication Technologies (GlobConPT)*, 2022.

[17] A. Jain, K. K. Gupta, S. K. Jain, P. Bhatnagar, "A bidirectional five-level buck PFC rectifier with wide output range for EV charging application," *IEEE Trans. Power Electron*, 37(11): 13439-13455, 2022.

[18] M. Eull, L. Zhou, M. Jahnes, M. Preindl, "Bidirectional nonisolated fast charger integrated in the electric vehicle traction drivetrain," *IEEE Trans. Transp. Electrifi.*, 8(1): 180-195, 2022.

[19] J. Gupta, B. Singh, "An on-board charging system for light EVs with G2V and V2G power transfer capability," in *Proc. IEEE IAS Global Conference on Emerging Technologies (GlobConET)*, 2022.

[20] S. Mukherjee, J. M. Ruiz, P. Barbosa, "A high power density wide range DC-DC converter for universal electric vehicle charging," *IEEE Trans. Power Electron*, 38(2): 1998-2012, 2023.

[21] H. Karneddi, D. Ronanki, "Universal bridgeless nonisolated battery charger with wide-output voltage range," *IEEE Trans. Power Electron*, 38(3): 2816-2820, 2023.

[22] H. Heydari-doostabad, T. O'Donnell, "A wide-range high-voltage-gain bidirectional DC-DC converter for V2G and G2V hybrid EV charger," *IEEE Trans. Ind. Electron*, 69(5): 4718-4729, 2021.

[23] D. Cittanti, M. Gregorio, E. Vico, E. Armando, R. Bojoi, "High performance digital multi-loop control of LLC resonant converters for EV fast charging with LUT-based feedforward and adaptive gain," *IEEE Trans. Ind. Appl.*, 58(5): 6266-6285, 2022.

[24] M. A. Alharbi, A. M. Alcaide, M. Dahidah, P. Montero-Robina, S. Ethni, V. Pickert, J. I. Leon, "Rotating phase shedding for interleaved DC-DC converter-based EVs fast DC chargers," *IEEE Trans. Power Electron*, 38(2): 1901-1909, 2023.

[25] L. Zhou, M. Jahnes, M. Eull, W. Wang, G. Cen, M. Preindl, "Robust control design for ride-through/trip of transformerless onboard bidirectional ev charger with variable-frequency critical-soft-switching," *IEEE Trans. Ind. Appl.*, 58(4): 4825-4837, 2022.

[26] R. Mayer, M. B. E. Kattel, S. V. G. Oliveira, "Multiphase interleaved bidirectional DC/DC converter with coupled inductor for electrified-vehicle applications," *IEEE Trans. Power Electron*, 36(3): 2533-2547, 2021.

[27] H. Moradisizkoohi, N. Elsayad, O. A. Mohammed, "A voltage-quadrupler interleaved bidirectional DC-DC converter with

intrinsic equal current sharing characteristic for electric vehicles," *IEEE Trans. Ind. Electron*, 68(2): 1803-1813, 2021.

[28] M. Abbasi, K. Kanathipan, J. Lam, "An interleaved bridgeless single-stage AC/DC converter with stacked switches configurations and soft-switching operation for high voltage EV battery systems," *IEEE Trans. Ind. Appl.*, 58(5): 5533-5545, 2022.

[29] R. Kushwaha, B. Singh, "A bridgeless isolated half bridge converter based EV charger with power factor pre-regulation," *IEEE Trans. Ind. Appl*, 58(3): 3967-3976, 2022.

[30] X. Zhou et al., "A high-efficiency high-power-density on-board low-voltage DC-DC converter for electric vehicles application," *IEEE Trans. Power Electron*, 36(11): 12781-12794, 2021.

Biographies



Farzad Sedaghati was born in Ardabil, Iran, in 1984. He received the M.S. and Ph.D. degrees both in Electrical Engineering in 2010 and 2014 from the University of Tabriz, Tabriz, Iran. In 2014, he joined the Faculty of Engineering, Mohaghegh Ardabili University, where he has been an Assistant Professor, since 2014. His current research interests include renewable energies and power electronic converters design and applications.

- Email: farzad.sedaghati@uma.ac.ir
- ORCID: [0000-0001-6974-4719](https://orcid.org/0000-0001-6974-4719)
- Web of Science Researcher ID: NA
- Scopus Author ID: 35410298600
- Homepage: <https://academics.uma.ac.ir/profiles?id=617>



Seyed Abbas Azimi was born in Ardabil, Iran, on February, 1996. He received his B.Sc. degree in Electrical Engineering from Islamic Azad University, Ardabil branch, Ardabil, Iran in 2018 and his M.Sc. degree in Power Electronics and electric machines engineering from the Azarbaijan Shahid Madani University, Tabriz, Iran in 2021. he is currently pursuing the Ph.D. degree in the Electrical Engineering at University of Mohaghegh Ardabili in Ardabil, Iran. His research interests include electric vehicle and power electronics design, simulation, modeling, and control of electrical machines.

- Email: abbasazimi@uma.ac.ir
- ORCID: [0009-0004-4886-2213](https://orcid.org/0009-0004-4886-2213)
- Web of Science Researcher ID: NA
- Scopus Author ID: 58975611100
- Homepage: NA

How to cite this paper:

F. Sedaghati, S. A. Azimi, "Electric vehicle battery charging using a non-isolated bidirectional DC-DC converter connected to t-type three level converter," *J. Electr. Comput. Eng. Innovations*, 13(1): 129-140, 2025.

DOI: [10.22061/jecei.2024.10870.743](https://doi.org/10.22061/jecei.2024.10870.743)

URL: https://jecei.sru.ac.ir/article_2205.html

